



Article

Ab Initio Study of Structural, Electronic and Magnetic Properties of $\text{TM}(\text{B}@\text{C}_{60})$ (TM = V, Cr) Sandwich Clusters and Infinite Molecular Wires

Jie Ji ¹, Tianxia Guo ¹, Liyan Qian ¹, Xiaokang Xu ¹, Huanning Yang ¹, Yue Xie ¹, Maoshuai He ², Xiaojing Yao ^{3,*}, Xiuyun Zhang ^{1,*} and Yongjun Liu ^{1,*}

¹ College of Physics Science and Technology, Yangzhou University, Yangzhou 225002, China

² College of Chemistry and Molecular Engineering, Qingdao University of Science and Technology, Qingdao 266042, China

³ College of Physics and Hebei Advanced Thin Film Laboratory, Hebei Normal University, Shijiazhuang 050024, China

* Correspondence: xjyao@hebtu.edu.cn (X.Y.); xyzhang@yzu.edu.cn (X.Z.); yjliu@yzu.edu.cn (Y.L.)

Abstract: The geometrical structure, electronic and magnetic properties of B-endoped C_{60} ($\text{B}@\text{C}_{60}$) ligand sandwich clusters, $\text{TM}(\text{B}@\text{C}_{60})_2$ (TM = V, Cr), and their one-dimensional (1D) infinite molecular wires, $[\text{TM}(\text{B}@\text{C}_{60})]_\infty$, have been systematically studied using first-principles calculations. The calculations showed that the TM atoms can bond strongly to the pentagonal (η^5 -coordinated) or hexagonal rings (η^6 -coordinated) of the endoped C_{60} ligands, with binding energies ranging from 1.90 to 3.81 eV. Compared to the configurations with contrast-bonding characters, the η^6 - and η^5 -coordinated bonding is energetically more favorable for V- $(\text{B}@\text{C}_{60})$ and Cr- $(\text{B}@\text{C}_{60})$ complexes, respectively. Interestingly, 1D infinite molecular wire $[\text{V}(\text{B}@\text{C}_{60})-\eta^6]_\infty$ is an antiferromagnetic half-metal, and 1D $[\text{Cr}(\text{B}@\text{C}_{60})-\eta^5]_\infty$ molecular wire is a ferromagnetic metal. The tunable electronic and magnetic properties of 1D $[\text{TM}(\text{B}@\text{C}_{60})]_\infty$ SMWs are found under compressive and tensile strains. These findings provide additional possibilities for the application of C_{60} -based sandwich compounds in electronic and spintronic devices.

Keywords: sandwich complexes; magnetic; density functional theory



Citation: Ji, J.; Guo, T.; Qian, L.; Xu, X.; Yang, H.; Xie, Y.; He, M.; Yao, X.; Zhang, X.; Liu, Y. Ab Initio Study of Structural, Electronic and Magnetic Properties of $\text{TM}(\text{B}@\text{C}_{60})$ (TM = V, Cr) Sandwich Clusters and Infinite Molecular Wires. *Nanomaterials* **2022**, *12*, 2770. <https://doi.org/10.3390/nano12162770>

Academic Editor: Nikos Tagmatarchis

Received: 18 July 2022

Accepted: 9 August 2022

Published: 12 August 2022

Publisher's Note: MDPI stays neutral with regard to jurisdictional claims in published maps and institutional affiliations.



Copyright: © 2022 by the authors. Licensee MDPI, Basel, Switzerland. This article is an open access article distributed under the terms and conditions of the Creative Commons Attribution (CC BY) license (<https://creativecommons.org/licenses/by/4.0/>).

1. Introduction

Since the discovery of C_{60} in 1985 [1,2], various fullerenes and their derivatives have attracted great attention due to their extraordinary stability and unique chemical and physical properties [3–7]. Particularly, versatile polygons, such as pentagons and hexagons, in fullerenes enabled them to be potential ligands bonding in external metal elements. Using a laser vaporization method, Nakajima et al. [8–10] successfully synthesized TM- C_{60} (TM = 3d transition metal) complexes in the 1990s, and predicted that the $\text{TM}_n(\text{C}_{60})_m$ clusters exhibit sandwich-like structures for $m = n + 1$, $n \leq 3$ or ring-like structures for $m = n$, $n > 3$. These structure characteristics were later confirmed via theoretical studies [11]. In addition, the TM- C_{60} coordinated bonds in $\text{TM}_n(\text{C}_{60})_m$ complexes were found to be dependent on the choice of TM atom [12,13]. However, differently from the comprehensively studied benzene (Bz)-ligand [10,14] or cyclopentadienyl (Cp)-ligand [15] sandwich complexes, most C_{60} sandwich complexes were confirmed to be non-magnetic or weakly magnetic [11–13], severely limiting their application in spintronic devices. Therefore, tuning the electronic and magnetic properties of fullerene-ligand sandwich complexes remains challenging.

Different from organic planar ligands (C_nH_n , $n = 5–8$) [16–22], the cage configuration of fullerenes enable their large spaces to accommodate other atoms or molecules for forming various core/shell complexes [23–32], which endows novel electronic properties on them and their TM-fullerene sandwich derivatives. For example, 1D infinite molecular

wires, $[TM\&(TM@C_{60})]_{\infty}$ (TM = Ti-Ni), composed of metallofullerene ($TM@C_{60}$) [23,33,34] and 3d TM atoms, were identified as displaying robust antiferromagnetic (AFM) semiconducting properties [20]. Unfortunately, the physical and chemical properties of sandwich isomers with different endoped fullerenes are rarely investigated. Herein, we explore the structure, electronic and magnetic properties of $TM(B@C_{60})_2$ (TM = V, Cr) sandwich clusters, as well as their 1D molecular wires (SMWs), $[TM\&(B@C_{60})]_{\infty}$, constructed by the fabricated core/shell structure, $B@C_{60}$ [35], as a building block. All the V-($B@C_{60}$) and Cr-($B@C_{60}$) sandwich complexes with η^6 - or η^5 - are thermodynamically stable, with high binding energies. Among them, the η^6 - and η^5 -coordinated bonding configurations are the stable ones, respectively, for the V and Cr atom. Moreover, 1D $[V\&(B@C_{60})-\eta^6]_{\infty}$ SMW is an antiferromagnetic half-metal, and 1D $[Cr\&(B@C_{60})-\eta^5]_{\infty}$ molecular wire is a ferromagnetic metal.

2. Models and Method

All the calculations were performed in the Vienna ab initio simulation package (VASP) [36,37] under the spin-polarized DFT framework. The exchange correlation interaction was described by the Perdew–Burke–Ernzerhof (PBE) [38] functional, and the interaction between valence electrons and ion nuclei was described by the projector–augmented wave potential (PAW) [39] method. In the process of calculations, the van der Waals (vdW) interaction was considered by using the DFT-D2 [40] method. In order to further consider the Coulomb interaction and exchange interactions of the *d*-electron in the transition metal atom, we adopted the GGA + U method [41], in which the parameter U was set to 3.0 eV [42,43]. In order to find the magnetic ground state of the 1D $[TM\&(B@C_{60})]_{\infty}$ SMWs, a $1 \times 1 \times 2$ supercell consisting of two TM atoms and two ($B@C_{60}$) units was used. The criteria for energy and atom force convergence were set to 10^{-4} eV and 0.01 eV/Å, respectively. To determine the magnetic ground states of the $TM\&(B@C_{60})$ clusters and molecular wires, diverse magnetic states with different magnetic moments were calculated and compared.

3. Results and Discussion

3.1. $TM\&(B@C_{60})_2$ (TM = V, Cr) Sandwich Clusters

First, we explored the structural characters of the endohedral $B@C_{60}$ cluster (see Figure 1a). Similar to the C_{60} molecule, the point group symmetry of the $B@C_{60}$ molecule is I_h , with the B atom sitting on the mass center of C_{60} . The diameter of $B@C_{60}$ is 7.09 Å and the C-C bond length is 1.45 Å. As shown in the spin density plot (see Figure 1b), the B atom in $B@C_{60}$ is spin-polarized with a local magnetic moment of 1.0 μ_B . The partial density of state (PDOS) of $B@C_{60}$ (Figure 1b) shows that the *p* states of the B atom is spin-polarized in the energy around the Fermi level, accounting for the 1.0 μ_B net magnetic moment. Two types of $TM\&(B@C_{60})_2$ configurations were considered: (i) $TM\&(B@C_{60})_2-\eta^5$, in which the sandwiched TM atoms are bonded to two pentagonal rings of two $B@C_{60}$ molecules forming η^5 -coordinate bonds; and (ii) $TM\&(B@C_{60})_2-\eta^6$, in which the TM atoms are bonded to two hexagonal rings of two $B@C_{60}$ s forming η^6 -coordinate bonds. Figure 1c,d show the optimized structures of $V\&(B@C_{60})_2$ and $Cr\&(B@C_{60})_2$. Clearly, all the $TM\&(B@C_{60})_2$ s favor normal sandwich configurations, with the TM atom sitting above the mass center of the pentagon or hexagon rings. For $V\&(B@C_{60})_2$, the η^6 coordinated configuration is more stable than the η^5 coordinated one, with an energy difference of 0.32 eV. On the contrary, the η^5 coordinated configuration is energetically more stable for $Cr\&(B@C_{60})_2$, with approximately 0.50 eV less energy.

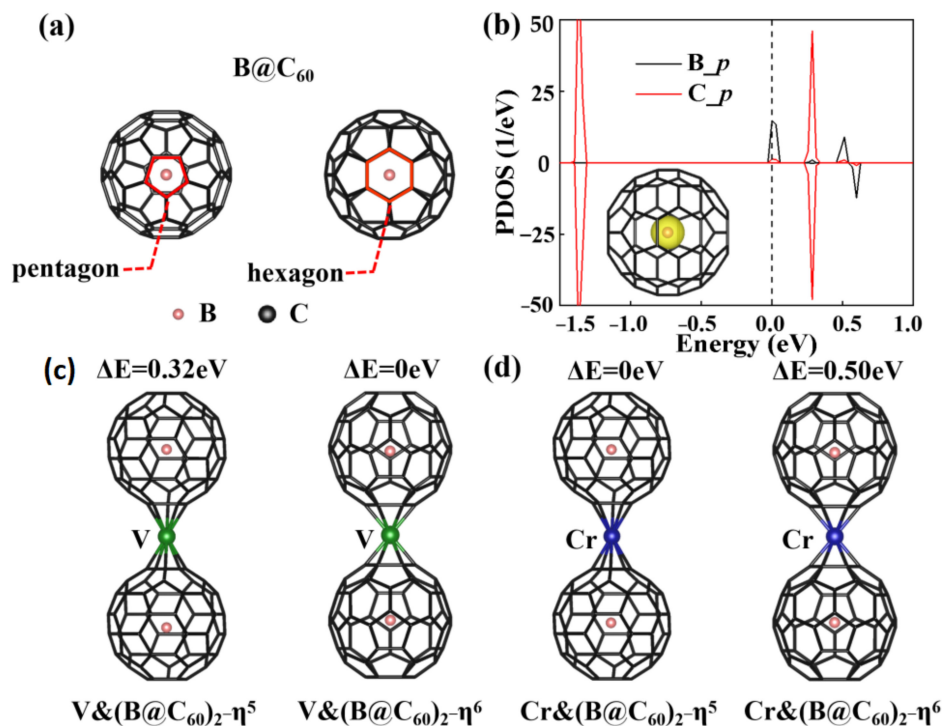


Figure 1. (a) Different views of B@C₆₀; (b) the PDOS and spin density plot of B@C₆₀ molecule; optimized structures of V&(B@C₆₀)₂ (c) and Cr&(B@C₆₀)₂ (d) with η^5 and η^6 bonding. ΔE is the energy difference between different bonding structures.

For V&(B@C₆₀)₂ and Cr&(B@C₆₀)₂, the distances of TM atoms from the mass center of the faced C_n ring ($n = 5, 6$) (d_{TM-C60}) to the nearest carbon rings are in the range of 1.73–2.00 Å (see Table 1), which are a bit larger than those in the TM-Bz (1.70 Å) [44], TM-Cp (1.72 Å–1.81 Å) [15] and TM-C₆₀ (1.75 Å) [6] sandwich compounds. In the compounds, the d_{TM-C60} s in η^5 coordinated systems are longer than those in the η^6 coordinated ones by around 0.21~0.28 Å. Moreover, the B atoms in the TM&(B@C₆₀)₂s (Figure 1c,d) deviate from the center of C₆₀ with 0.02~0.08 Å (see Table 1). In order to investigate the stability of these TM&(B@C₆₀)₂ sandwich clusters, the binding energies (E_b) are calculated based on the following formula:

$$E_b = E_{TM\&(B@C60)2} - [E_{TM} + 2E_{B@C60}] \quad (1)$$

where E_{TM} , $E_{B@C60}$ and $E_{TM\&(B@C60)2}$ are the energies of the isolated TM atom, B@C₆₀ molecule and TM&(B@C₆₀)₂, respectively. Shown in Table 1, the E_b s of V&(B@C₆₀)₂ and Cr&(B@C₆₀)₂ with η^5/η^6 coordinated bonding are approximately $-1.90/-2.23 \text{ eV}$ and $-3.81/-3.31 \text{ eV}$, respectively, implying that these sandwich clusters are energetically stable. Figure 2 plots the PDOS of the TM&(B@C₆₀)₂ (TM = Ti, V) clusters to explore the physical origin of their stability. For V&(B@C₆₀)₂- η^6 , strong C-*p* and V-*d*_{*x*²-*y*²} orbitals hybridization are observed in the energy window of [−0.75, −0.60 eV], and the hybridization between B-*p* and V-*d*_{*z*²} states are in the energy window of [−0.25, 0 eV] (see Figure 2b) below the Fermi level. While in the case of V&(B@C₆₀)₂- η^5 , relatively weaker B-*p* and V-*d*_{*z*²} hybridization is found (see Figure 2a), which is responsible for its low stability. In Cr&(B@C₆₀)₂- η^6 , the hybridization between C-*p* orbitals and Cr-*d*_{*x*²-*y*²}, *d*_{*z*²} orbitals is observed in the energy of [−0.5, −0.1 eV]. In contrast, for Cr&(B@C₆₀)₂- η^5 , stronger *d*-*p* hybridization is found deep in the energy window below the Fermi level, around [−1.3, −1.2 eV] and [−0.6, −0.4 eV]. As a result, the most energetically stable configuration is Cr&(B@C₆₀)₂- η^5 .

Table 1. Optimized lattice constant (L , Å), local magnetic moment of TM atom and B atom (LMM, μ_B), binding energy (E_b , eV), the Bader charge (Δe , e) transferred from TM atom to B@C₆₀ molecule, distance of TM atom to the mass center of faced C_n rings (d_{TM-C60}), distance of B atom to the mass center of the nearest η^5 - or η^6 -carbon ring in C₆₀ (d_{B-C60} , Å), deviations of the encapsulated B atom to the mass center of C₆₀ molecule (Δh , Å).

Sys	L(Å)	LMM(μ_B)		E_b (eV)	Δe (e)	d_{TM-C60} (Å)	d_{B-C60} (Å)	Δh (Å)
		TM	B					
V&(B@C ₆₀) ₂ - η^5	—	3.00	0.41	−1.90	1.13	1.96	3.28–3.53	0.03
V&(B@C ₆₀) ₂ - η^6	—	1.00	0.41	−2.23	1.30	1.73	3.12–3.21	0.02
Cr&(B@C ₆₀) ₂ - η^5	—	6.00	0.42	−3.81	1.09	2.00	3.24	0.08
Cr&(B@C ₆₀) ₂ - η^6	—	2.00	0.41	−3.31	1.00	1.73	3.10–3.22	0.03
[V&(B@C ₆₀) ₂ - η^5] _∞	9.84	1.00	0.41	−5.24	0.32	1.69	3.46–3.40	0.32
[Cr&(B@C ₆₀) ₂ - η^5] _∞	10.64	4.00	0.41	−8.67	0.09	2.01	3.31–3.32	0.08

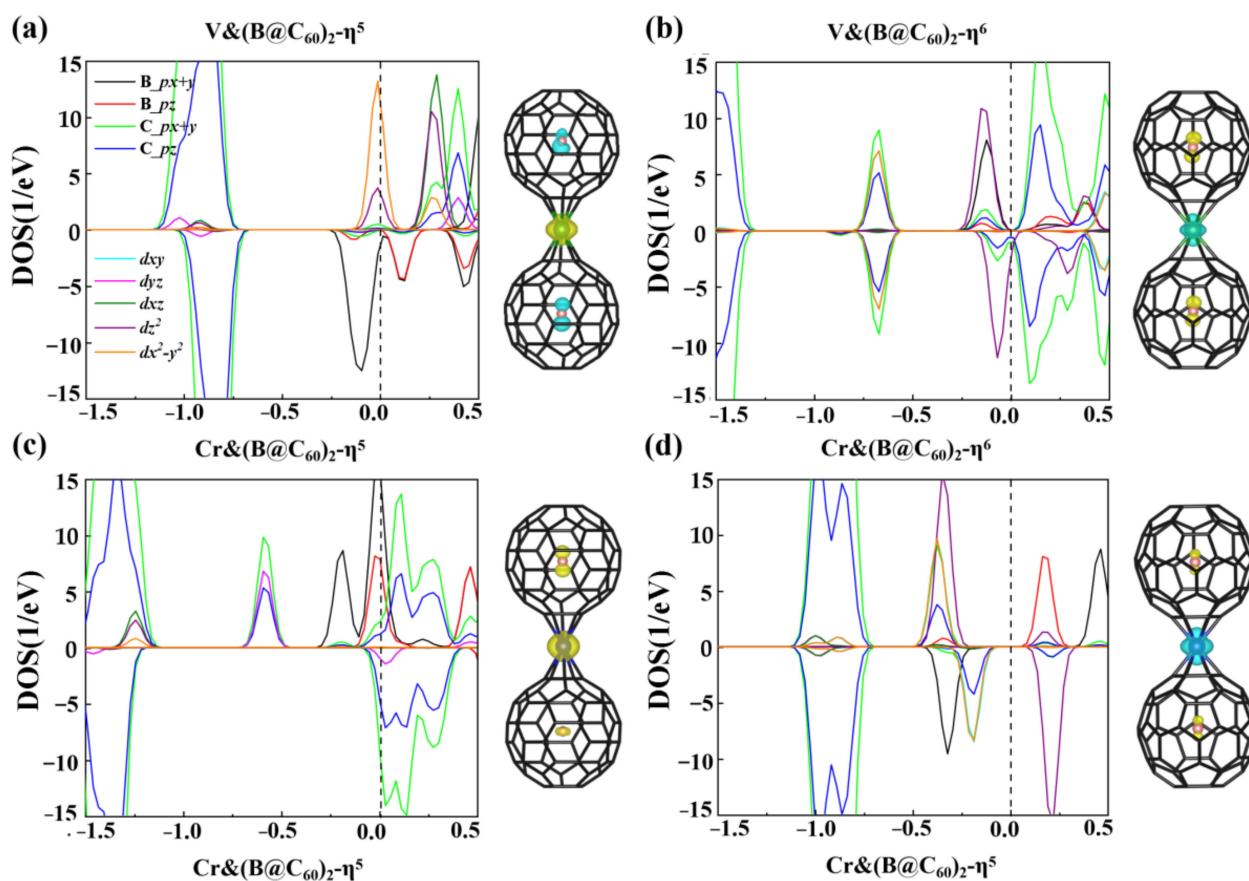


Figure 2. The spin density and PDOS of V&(B@C₆₀)₂ (a,b) and Cr&(B@C₆₀)₂ (c,d).

To determine the magnetic ground states of these TM&(B@C₆₀)₂ clusters, we considered different spin states for each system (see Table S1 in the supporting information, SI). For V&(B@C₆₀)₂, the magnetic moment of its ground state is 3.0 μ_B and 1.0 μ_B in their η^5/η^6 coordinated configurations. Their second lower-energy isomers are found to have magnetic moments of 5.0 μ_B and 3.0 μ_B , which are less stable than the ground states by approximately 0.01 eV and are 0.03 eV higher in energy, respectively. In addition, for Cr&(B@C₆₀)₂- η^5 and Cr&(B@C₆₀)₂- η^6 , the magnetic moment of 6.0 μ_B and 2.0 μ_B is observed for their ground states, which are approximately 0.03 eV and 0.17 eV lower in energy, respectively, than their second higher-energy isomers with the same magnetic moment of 4.0 μ_B . The inset in Figure 2 shows the spin densities of V&(B@C₆₀)₂ and Cr&(B@C₆₀)₂. Clearly, the magnetic moments of both systems are mainly contributed to the B atoms and TM atoms. The B atom

and TM atom for $V\&(B@C_{60})_2-\eta^5$ and $Cr\&(B@C_{60})_2-\eta^6$ contribute to opposite spins. In contrast, the same spins are found for the B atom and Cr atom in $Cr\&(B@C_{60})_2-\eta^5$. As for $V\&(B@C_{60})_2-\eta^6$, its magnetic moments mainly arise from two B atoms with opposite spins.

3.2. D infinite $[TM\&(B@C_{60})]_{\infty}$ ($TM = V, Cr$) SMWs

Figure 3a,b show the optimized structures of 1D $[V\&(B@C_{60})]_{\infty}$ and $[Cr\&(B@C_{60})]_{\infty}$. Here, respective 1D $[V\&(B@C_{60})]_{\infty}$ and $[Cr\&(B@C_{60})]_{\infty}$ with η^6 - and η^5 -coordinated configurations are considered. Similar to the $TM\&(B@C_{60})_2$ clusters, both 1D $[TM\&(B@C_{60})]_{\infty}$ SMWs have normal sandwich structures. The lattice constants of 1D $[V\&(B@C_{60})-\eta^6]_{\infty}$ and $[Cr\&(B@C_{60})-\eta^5]_{\infty}$ SMWs are 9.84 Å and 10.64 Å, respectively (see Table 1 and Figure 3a,b). Meanwhile, B atoms in the endoped C_{60} are separate from the mass center of C_{60} , with the deviation values (Δh) of 0.32 Å and 0.09 Å, respectively. Table 1 shows that the d_{TM-C60} in 1D $[V\&(B@C_{60})-\eta^6]_{\infty}$ SMW and $[Cr\&(B@C_{60})-\eta^5]_{\infty}$ SMW are approximately 1.70 Å and 2.01 Å, respectively, and are a bit shorter than that in the finite sandwich clusters.

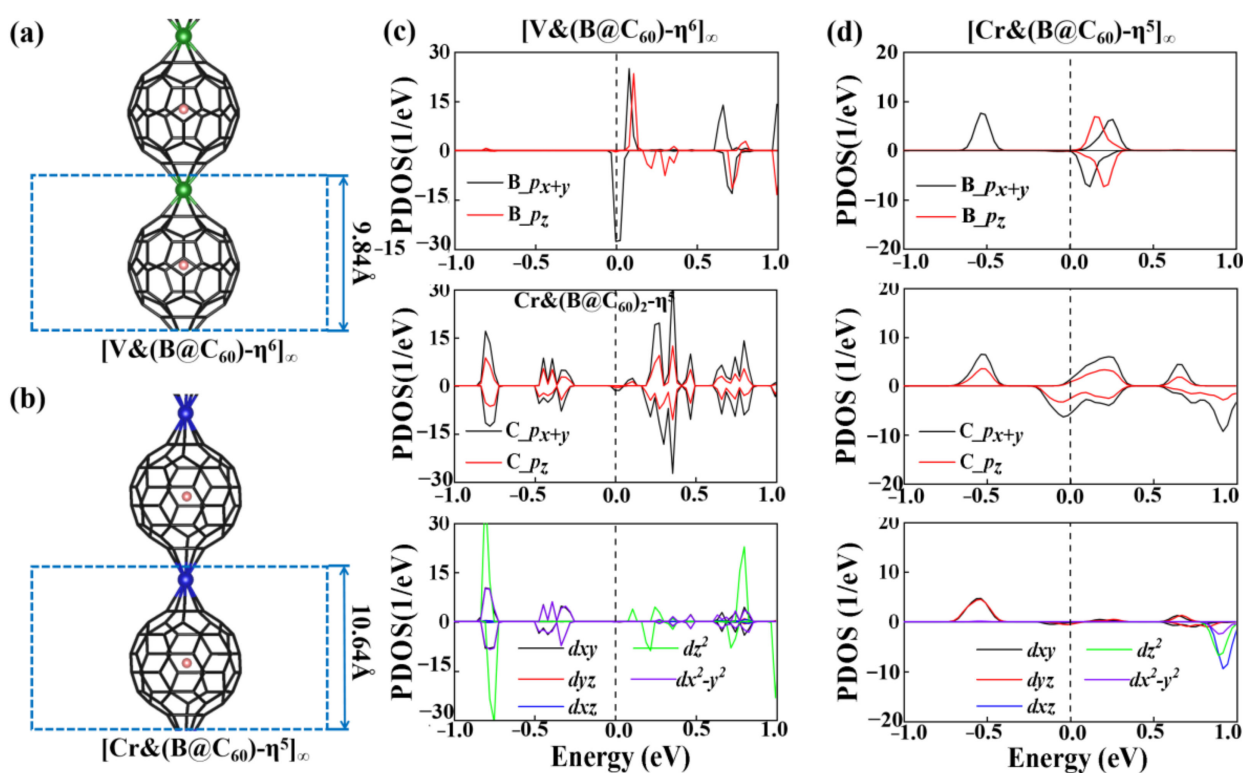


Figure 3. The optimized structures (a,b) and PDOS (c,d) of 1D $[V\&(B@C_{60})-\eta^6]_{\infty}$ and $[Cr\&(B@C_{60})-\eta^5]_{\infty}$ SMWs.

To evaluate the stability of these SMWs, we defined the binding energy (E_b) of SMWs as:

$$E_b = E_{[TM\&(B@C_{60})]_{\infty}} - E_{TM} - E_{B@C_{60}} \quad (2)$$

where $E_{[TM\&(B@C_{60})]_{\infty}}$, E_{TM} and $E_{B@C_{60}}$ are the energies of $[TM\&(B@C_{60})]_{\infty}$ SMWs, $3d$ TM atoms and $B@C_{60}$ ligand, respectively. As shown in Table 1, the binding energies of $[V\&(B@C_{60})-\eta^6]_{\infty}$ and $[Cr\&(B@C_{60})-\eta^5]_{\infty}$ are about -5.24 eV and -8.67 eV, respectively, larger than that of the reported 1D organometallic and non-organometallic SMWs [15,22,45–47]. The Bader charge calculations indicate that their high stability is correlated with charge transfer from the TM atom to $B@C_{60}$ molecule, which is about 1.22e and 1.09 e for V and Cr, respectively. Figure 3c,d present the PDOS of 1D $[V\&(B@C_{60})-\eta^6]_{\infty}$ SMW and $[Cr\&(B@C_{60})-\eta^5]_{\infty}$ SMW. Strong hybridization between C- p and V- d_{z^2} , $d_{x^2-y^2}$ orbitals are found in 1D $[V\&(B@C_{60})-\eta^6]_{\infty}$ SMW. As shown in Figure 4d, C- p and Cr- dyz of $[Cr\&(B@C_{60})-\eta^5]_{\infty}$ SMW are strongly hybridized.

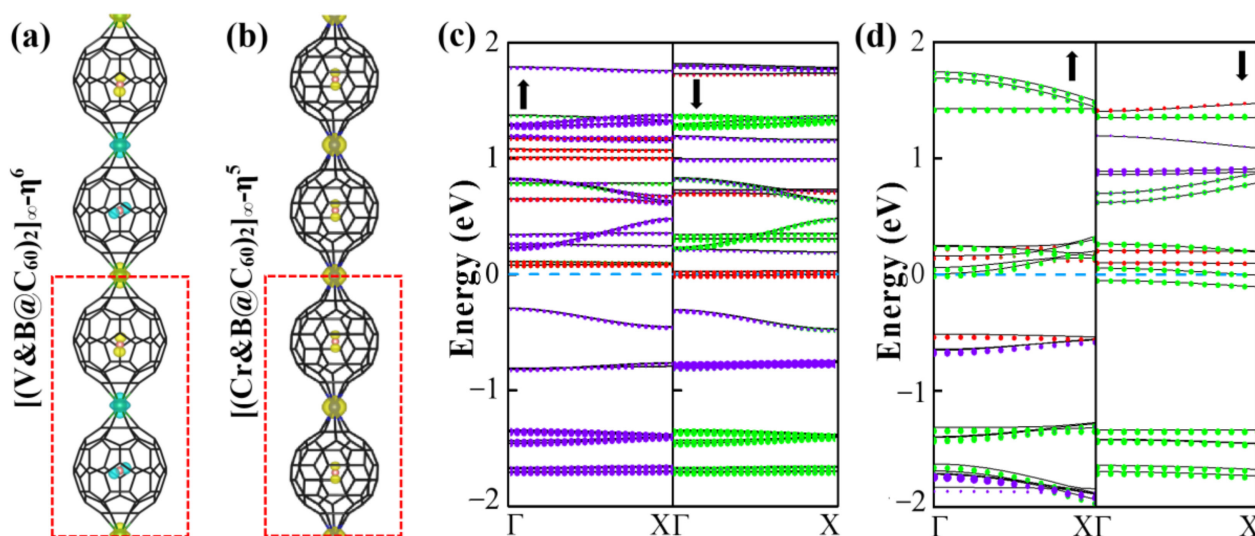


Figure 4. Spin densities (a,b) and decomposed band structures (c,d) of 1D $[V\&(B@C_{60})-\eta^6]_{\infty}$ and (b) $[Cr\&(B@C_{60})-\eta^5]_{\infty}$ SMWs, yellow and blue colors indicate up and down spins, respectively. red, green and violet colors represent B-*p*, C-*p* and TM-*d* orbitals, respectively, the size of the color balls is proportion to the contributions from the states.

Furthermore, to determine the magnetic ground state of 1D $[V\&(B@C_{60})-\eta^6]_{\infty}$ and $[Cr\&(B@C_{60})-\eta^5]_{\infty}$ SMWs, a double cell was constructed to explore their FM and AFM configurations (see Figure 4a,b). Obviously, 1D $[V\&(B@C_{60})-\eta^6]_{\infty}$ SMW favors an AFM ground state, in which two nearby V-B atoms (V-B dimer) FM couple with each other, while AFM couples with its nearby dimer (see Figure 4a). The FM state is less stable by approximately 0.35 eV higher in energy. On the contrary, 1D $[Cr\&(B@C_{60})-\eta^5]_{\infty}$ SMW has a FM ground state, which is more stable than the AFM state by approximately 0.10 eV lower in energy (see Table S2). Moreover, 1D $[V\&(B@C_{60})-\eta^6]_{\infty}$ SWM is found to be an AFM half-metal, in which the spin-up and spin-down electronic states are semiconducting and conducting, respectively (see Figure 4c), while 1D $[Cr\&(B@C_{60})-\eta^5]_{\infty}$ SMW is a FM metal (see Figure 4d). Finally, we explored the electronic and magnetic properties of the most stable 1D $[TM\&(B@C_{60})-\eta^5]_{\infty}$ (TM = V, Cr) SMWs under external strains. For 1D $[V\&(B@C_{60})-\eta^6]_{\infty}$ SMW, it undergoes an AFM HM-AFM semiconductor (SC) transition under 5% and 10% compressive strain (see Figure 5a,b and Table 2). On the contrary, it is changed to a FM metal under 5% and 10% tensile strain (see Figure 5c,d and Table 2). In addition, 1D $[Cr\&(B@C_{60})-\eta^5]_{\infty}$ SMW transfers to both a FM metal and a ferrimagnetic (FIM) metal under 5% compressive strain and 5% (10%) tensile strain (see Figure 5f-h and Table 2), respectively, and changes to an AFM metal under 10% compressive strain (see Figure 5e and Table 2).

Table 2. Local magnetic moment of TM atom and B atom (LMM, μ_B) under different strain.

Sys		LMM(μ_B)			
		$\epsilon = -10\%$	$\epsilon = -5\%$	$\epsilon = +5\%$	$\epsilon = +10\%$
$[V\&(B@C_{60})-\eta^6]_{\infty}$	V	1.31/−1.33	1.00/−0.97	1.83/1.83	2.75/2.75
	B	0.36/−0.35	0.41/−0.42	0.42/0.42	0.42/0.42
$[Cr\&(B@C_{60})-\eta^5]_{\infty}$	Cr	2.85/−2.92	3.12/3.12	4.03/4.03	4.25/4.25
	B	0.38/0.38	0.37/0.37	−0.42/−0.42	−0.32/−0.32

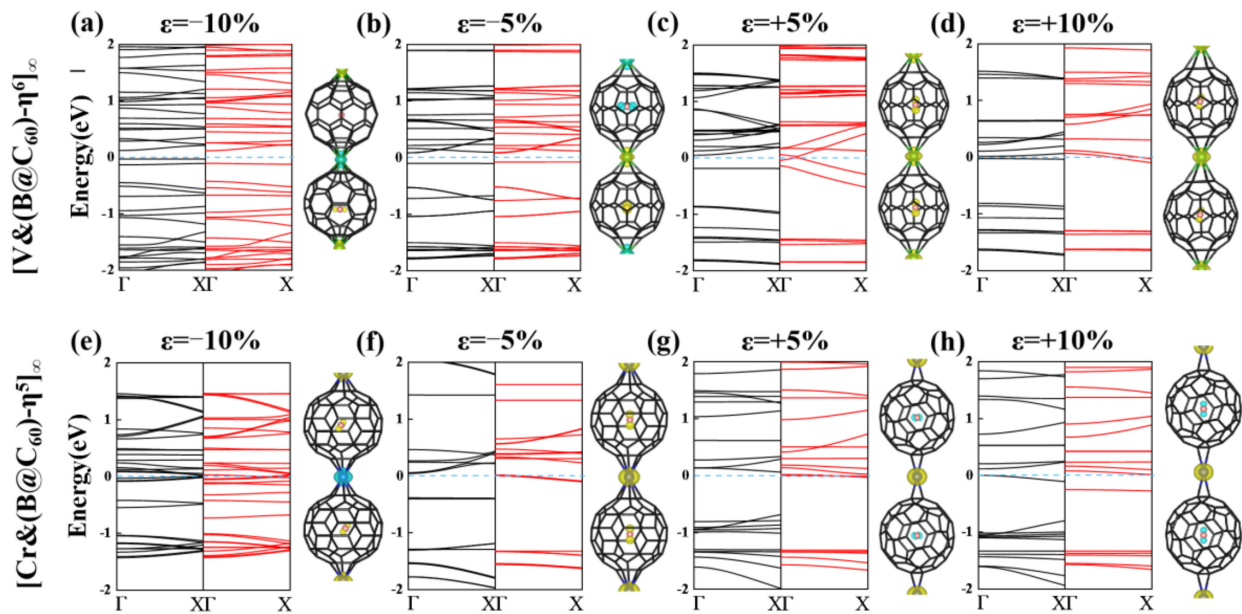


Figure 5. Band structures and spin density of 1D $[V\&(B@C_{60})-\eta^6]_{\infty}$ and $[Cr\&(B@C_{60})-\eta^5]_{\infty}$ SMWs under several strains of -10% (a,e), -5% (b,f), $+5\%$ (c,g) and $+10\%$ (d,h); yellow and blue colors indicate up and down spins, respectively. The blue, black and red lines represent the Fermi level, the spin up and spin down electronic bands, respectively.

4. Conclusions

Using first principles calculations, we systematically investigated the structure, electronic and magnetic properties of $3d$ transition metal atoms and $B@C_{60}$ sandwich clusters, $TM\&(B@C_{60})_2$ ($TM = V, Cr$), and their 1D infinite SMWs, $[TM\&(B@C_{60})]_{\infty}$. Our results showed that all the studied systems possess normal sandwich structures with extremely thermodynamic stabilities. It was found that respective η^6 - and η^5 -bonding configurations are confirmed for the systems with $TM = V$ and Cr . One-dimensional $[V\&(B@C_{60})-\eta^6]_{\infty}$ and $[Cr\&(B@C_{60})-\eta^5]_{\infty}$ SMWs are an antiferromagnetic half-metal and a ferromagnetic metal. Furthermore, the magnetic properties can be modulated by exerting biaxial compressive and tensile strains. Finally, we should state that the diverse electronic and magnetic properties of the studied complexes may be highly sensitive to their surroundings [48,49]. Therefore, exploring their performance in a complicated environment, instead of non-free-standing states, is also of importance.

Supplementary Materials: The following supporting information can be downloaded at: <https://www.mdpi.com/article/10.3390/nano12162770/s1>, Table S1. Different spin states for each system. Table S2. The energy difference between FM and AFM states. Atomic coordination of $V\&(B@C_{60})_2-\eta^5$. Atomic coordination of $V\&(B@C_{60})_2-\eta^6$. Atomic coordination of $Cr\&(B@C_{60})_2-\eta^5$. Atomic coordination of $Cr\&(B@C_{60})_2-\eta^6$. Atomic coordination of $[V\&(B@C_{60})-\eta^6]_{\infty}$. Atomic coordination of $[Cr\&(B@C_{60})-\eta^5]_{\infty}$.

Author Contributions: J.J., T.G. and L.Q. contributed equally to this work. Investigation, data analysis, and writing—original draft, J.J., T.G. and L.Q.; investigation, X.X., H.Y. and Y.X.; investigation, writing—review and editing, M.H.; review and editing, X.Y. and Y.L.; supervision, X.Z. All authors have read and agreed to the published version of the manuscript.

Funding: This work is supported by the NSFC (12004098), the Open Funds of the State Key Laboratory of Rare Earth Resource Utilization (RERU2021011), Science and Technology Project of Hebei Education Department (QN2020157). We thank the computational resources at Yangzhou University and Hebei Normal University.

Conflicts of Interest: The authors declare no conflict of interest.

References

1. Kroto, H.W.; Heath, J.R.; O'Brien, S.C.; Curl, R.F.; Smalley, R.E. C₆₀: Buckminsterfullerene. *Nature* **1985**, *318*, 162–163. [[CrossRef](#)]
2. Scott, L.T.; Boorum, M.M.; McMahon, B.J.; Hagen, S.; Mack, J.; Blank, J.; Wegner, H.; de Meijere, A. A Rational Chemical Synthesis of C₆₀. *Science* **2002**, *295*, 1500–1503. [[CrossRef](#)] [[PubMed](#)]
3. Goulart, M.; Kuhn, M.; Martini, P.; Chen, L.; Hagelberg, F.; Kaiser, A.; Scheier, P.; Ellis, A.M. Highly Stable [C₆₀AuC₆₀]^{+/-} Dumbbells. *J. Phys. Chem. Lett.* **2018**, *9*, 2703–2706. [[CrossRef](#)]
4. Lee, K.; Choi, B.; Plante, I.J.-L.; Paley, M.V.; Zhong, X.; Crowther, A.C.; Owen, J.S.; Zhu, X.; Roy, X. Two-Dimensional Fullerene Assembly from an Exfoliated Van Der Waals Template. *Angew. Chem. Int. Ed.* **2018**, *57*, 6125–6129. [[CrossRef](#)]
5. Mararov, V.V.; Utas, T.V.; Bondarenko, L.V.; Tupchaya, A.Y.; Vekovshinin, Y.E.; Gruznev, D.V.; Mihalyuk, A.N.; Zotov, A.V.; Saranin, A.A. Self-Assembly of C₆₀ Layers at Ti/NiSi₂ Atomic Sandwich on Si(111). *Surf. Sci.* **2022**, *715*, 121934. [[CrossRef](#)]
6. Rekhviashvili, S.S.; Bukhurova, M.M. Equilibrium Parameters for Bilayer Graphene Filled with Fullerene C₆₀ Molecules. *Tech. Phys. Lett.* **2021**, *47*, 403–404. [[CrossRef](#)]
7. Talmazan, R.A.; Liedl, K.R.; Krautler, B.; Podewitz, M. The Intermolecular Anthracene-Transfer in a Regiospecific Antipodal C₆₀ Difunctionalization. *Org. Biomol. Chem.* **2020**, *18*, 4090–4103. [[CrossRef](#)] [[PubMed](#)]
8. Nakajima, A.; Nagao, S.; Takeda, H.; Kurikawa, T.; Kaya, K. Multiple Dumbbell Structures of Vanadium–C₆₀ Clusters. *J. Chem. Phys.* **1997**, *107*, 6491–6494. [[CrossRef](#)]
9. Nagao, S.; Kurikawa, T.; Miyajima, K.; Nakajima, A.; Kaya, K. Formation and Structures of Transition Metal–C₆₀ Clusters. *J. Phys. Chem. A* **1998**, *102*, 4495–4500. [[CrossRef](#)]
10. Nakajima, A.; Kaya, K. A Novel Network Structure of Organometallic Clusters in the Gas Phase. *J. Phys. Chem. A* **2000**, *104*, 176–191. [[CrossRef](#)]
11. Zhang, X.; Wang, J.; Zeng, X.C. Ab Initio Study of Structural, Electronic, and Magnetic Properties of V_n(C₆₀)_m Complexes. *J. Phys. Chem. A* **2009**, *113*, 5406–5413. [[CrossRef](#)] [[PubMed](#)]
12. Andriotis, A.N.; Menon, M. Geometry and Bonding in Small (C₆₀)_nNi_m Clusters. *Phys. Rev. B* **1999**, *60*, 4521–4524. [[CrossRef](#)]
13. Andriotis, A.N.; Menon, M.; Froudakis, G.E. Contrasting Bonding Behaviors of 3d Transition Metal Atoms with Graphite and C₆₀. *Phys. Rev. B* **2000**, *62*, 9867–9871. [[CrossRef](#)]
14. Judai, K.; Hirano, M.; Kawamata, H.; Yabushita, S.; Nakajima, A.; Kaya, K. Formation of Vanadium-Arene Complex Anions and Their Photoelectron Spectroscopy. *Chem. Phys. Lett.* **1997**, *270*, 23–30. [[CrossRef](#)]
15. Shen, L.; Yang, S.-W.; Ng, M.-F.; Ligatchev, V.; Zhou, L.; Feng, Y. Charge-Transfer-Based Mechanism for Half-Metallicity and Ferromagnetism in One-Dimensional Organometallic Sandwich Molecular Wires. *J. Am. Chem. Soc.* **2008**, *130*, 13956–13960. [[CrossRef](#)] [[PubMed](#)]
16. Liu, X.; Tan, Y.; Zhang, G.; Pei, Y. Electronic Structure and Spin Transport Properties of a New Class of Semiconductor Surface-Confined One-Dimensional Half-Metallic Eu(C_nH_{n-2})_N (N=7–9) Sandwich Compounds and Molecular Wires: First Principle Studies. *J. Phys. Chem. C* **2018**, *122*, 16168–16177. [[CrossRef](#)]
17. Wang, C.H.; Xu, L.F.; Fan, X.-L.; Wang, J.-T. Structural Stability and Electronic Property of Sandwich Clusters (C_mH_m)Mn(C_nH_n) (m, n=5,6) Following an 18-Electron Principle. *Phys. Lett. A* **2011**, *375*, 562–567. [[CrossRef](#)]
18. Shao, P.; Ding, L.P.; Luo, D.-B.; Lu, C. Probing the Structures, Electronic and Bonding Properties of Multidecker Lanthanides: Neutral and Anionic Ln_n(COT)_n (Ln = Ce, Nd, Eu, Ho and Yb; n, m = 1, 2) Complexes. *J. Mol. Graph. Model.* **2019**, *90*, 226–234.
19. Zhang, X.; Liu, Y. Tunable Electronic and Magnetic Properties of Transition Metal-Cyclopentadiene Sandwich Molecule Wires Functionalized Narrow Single Wall Carbon Nanotubes. *J. Phys. Chem. C* **2016**, *120*, 19812–19820. [[CrossRef](#)]
20. Zhang, X.; Gong, X.; Sun, Y.; Xu, M.; Xi, B.; Zhao, X.; Ye, X.; Yao, X.; He, M.; Liu, L.; et al. 3d Transition Metal-Metallofullerene-Ligand Molecular Wires: Robust One-Dimensional Antiferromagnetic Semiconductors. *J. Phys. Chem. C* **2019**, *123*, 30571–30577. [[CrossRef](#)]
21. Lu, K.; Gao, W.; Xu, M.; Sun, Y.; Li, J.; Yao, X.; Liu, Y.; Zhang, X. Spin Transport Properties of One-Dimensional Benzene Ligand Organobimetallic Sandwich Molecular Wires. *ACS Omega* **2020**, *5*, 5534–5539. [[CrossRef](#)] [[PubMed](#)]
22. Gao, W.; Yao, X.; Sun, Y.; Sun, W.; Liu, H.; Liu, J.; Liu, Y.; Zhang, X. Theoretical Study on Sandwich-Like Transition-Metal-Cyclooctatetraene Clusters and One-Dimensional Infinite Molecular Wires. *ACS Omega* **2019**, *4*, 9739–9744. [[CrossRef](#)] [[PubMed](#)]
23. Liu, S.; Sun, S. Recent Progress in the Studies of Endohedral Metallofullerenes. *J. Organomet. Chem.* **2000**, *599*, 74–86. [[CrossRef](#)]
24. Bethune, D.S.; Johnson, R.D.; Salem, J.R.; de Vries, M.S.; Yannoni, C.S. Atoms in Carbon Cages: The Structure and Properties of Endohedral Fullerenes. *Nature* **1993**, *366*, 123–128. [[CrossRef](#)]
25. Arie, A.A.; Lee, J.K. Effect of Boron Doped Fullerene C₆₀ Film Coating on the Electrochemical Characteristics of Silicon Thin Film Anodes for Lithium Secondary Batteries. *Synth. Met.* **2011**, *161*, 158–165. [[CrossRef](#)]
26. Das, P.; Chattaraj, P.K. Comparison between Electride Characteristics of Li₃@B₄₀ and Li₃@C₆₀. *Front. Chem.* **2021**, *9*, 638581. [[CrossRef](#)] [[PubMed](#)]
27. Das, P.; Saha, R.; Chattaraj, P.K. Encapsulation of Mg₂ inside a C₆₀ Cage Forms an Electride. *J. Comput. Chem.* **2020**, *41*, 1645–1653. [[CrossRef](#)] [[PubMed](#)]
28. Feng, L.; Hao, Y.; Liu, A.; Slanina, Z. Trapping Metallic Oxide Clusters inside Fullerene Cages. *Acc. Chem. Res.* **2019**, *52*, 1802–1811. [[CrossRef](#)] [[PubMed](#)]
29. Koi, N.; Oku, T. Molecular Orbital Calculations of Hydrogen Storage in Carbon and Boron Nitride Clusters. *Sci. Technol. Adv. Mater.* **2004**, *5*, 625–628. [[CrossRef](#)]
30. Kurotobi, K.; Murata, Y. A Single Molecule of Water Encapsulated in Fullerene C₆₀. *Science* **2011**, *333*, 613–616. [[CrossRef](#)]

31. Ren, Y.X.; Ng, T.Y.; Liew, K.M. State of Hydrogen Molecules Confined in C₆₀ Fullerene and Carbon Nanocapsule Structures. *Carbon* **2006**, *44*, 397–406. [[CrossRef](#)]
32. Tishchenko, O.; Truhlar, D.G. Atom-Cage Charge Transfer in Endohedral Metallofullerenes: Trapping Atoms within a Sphere-Like Ridge of Avoided Crossings. *J. Phys. Chem. Lett.* **2013**, *4*, 422–425. [[CrossRef](#)]
33. Bolskar, R.D.; Benedetto, A.F.; Husebo, L.O.; Price, R.E.; Jackson, E.F.; Wallace, S.; Wilson, L.J.; Alford, J.M. First Soluble M@C₆₀ Derivatives Provide Enhanced Access to Metallofullerenes and Permit in Vivo Evaluation of Gd@C₆₀[C(COOH)₂]₁₀ as a MRI Contrast Agent. *J. Am. Chem. Soc.* **2003**, *125*, 5471–5478. [[CrossRef](#)] [[PubMed](#)]
34. Shinohara, H. Endohedral Metallofullerenes. *Rep. Prog. Phys.* **2000**, *63*, 843–892. [[CrossRef](#)]
35. Zou, Y.J.; Zhang, X.W.; Li, Y.L.; Wang, B.; Yan, H.; Cui, J.Z.; Liu, L.M.; Da, D.A. Bonding Character of the Boron-Doped C₆₀ Films Prepared by Radio Frequency Plasma Assisted Vapor Deposition. *J. Mater. Sci.* **2002**, *37*, 1043–1047. [[CrossRef](#)]
36. Kresse, G.; Hafner, J.J.P.R.B. Initio Molecular Dynamics for Open-Shell Transition Metals. *Phys. Rev. B Condens. Matter Phys.* **1993**, *48*, 13115–13118. [[CrossRef](#)] [[PubMed](#)]
37. Kresse, G.; Furthmüller, J. Efficiency of Ab-Initio Total Energy Calculations for Metals and Semiconductors Using a Plane-Wave Basis Set. *Comput. Mater. Sci.* **1996**, *6*, 15–50. [[CrossRef](#)]
38. Perdew, J.P.; Burke, K.; Ernzerhof, M. Generalized Gradient Approximation Made Simple. *Phys. Rev. Lett.* **1996**, *77*, 3865–3868. [[CrossRef](#)]
39. Blöchl, P.E. Projector Augmented-Wave Method. *Phys. Rev. B* **1994**, *50*, 17953–17979. [[CrossRef](#)]
40. Grimme, S. Semiempirical GGA-Type Density Functional Constructed with a Long-Range Dispersion Correction. *J. Comput. Chem.* **2006**, *27*, 1787–1799. [[CrossRef](#)]
41. Xiang, H.; Dronskowski, R.; Eck, B.; Tchougréeff, A.L. Electronic and Magnetic Structure of Transition-Metal Carbodiimides by Means of GGA+U Theory. *J. Phys. Chem. A* **2010**, *114*, 12345–12352. [[CrossRef](#)] [[PubMed](#)]
42. Wehling, T.O.; Lichtenstein, A.I.; Katsnelson, M.I. Transition-Metal Adatoms on Graphene: Influence of Local Coulomb Interactions on Chemical Bonding and Magnetic Moments. *Phys. Rev. B* **2011**, *84*, 235110. [[CrossRef](#)]
43. Li, S.; Ao, Z.M.; Zhu, J.J.; Ren, J.C.; Yi, J.B.; Wang, G.X.; Liu, W. Strain Controlled Ferromagnetic-Antiferromagnetic Transformation in Mn-Doped Silicene for Information Transformation Devices. *J. Phys. Chem. Lett.* **2017**, *8*, 1484–1488. [[CrossRef](#)]
44. Maslyuk, V.V.; Bagrets, A.; Meded, V.; Arnold, A.; Evers, F.; Brandbyge, M.; Bredow, T.; Mertig, I. Organometallic Benzene-Vanadium Wire: A One-Dimensional Half-Metallic Ferromagnet. *Phys. Rev. Lett.* **2006**, *97*, 097201. [[CrossRef](#)] [[PubMed](#)]
45. Wang, J.; Acioli, P.H.; Jellinek, J. Structure and Magnetism of V_nBz_{n+1} Sandwich Clusters. *J. Am. Chem. Soc.* **2005**, *127*, 2812–2813. [[CrossRef](#)] [[PubMed](#)]
46. Zhang, X.; Ng, M.-F.; Wang, Y.; Wang, J.; Yang, S.-W. Theoretical Studies on Structural, Magnetic, and Spintronic Characteristics of Sandwiched Eu_nCOT_{n+1} (n = 1–4) Clusters. *ACS Nano* **2009**, *3*, 2515–2522. [[CrossRef](#)] [[PubMed](#)]
47. Xiang, H.; Yang, J.; Hou, J.G.; Zhu, Q. One-Dimensional Transition Metal–Benzene Sandwich Polymers: Possible Ideal Conductors for Spin Transport. *J. Am. Chem. Soc.* **2006**, *128*, 2310–2314. [[CrossRef](#)] [[PubMed](#)]
48. Jacak, W.; Krasnyj, J.; Jacak, L. Reducing of Magnon-Induced Spin Pure Dephasing in Quantum Dots at Low Temperatures. *Phys. Rev. B* **2008**, *78*, 073303. [[CrossRef](#)]
49. Jacak, L.; Krasnyj, J.; Jacak, W.; Gonczarek, R.; Machnikowski, P. Unavoidable Decoherence in Semiconductor Quantum Dots. *Phys. Rev. B* **2005**, *72*, 245309. [[CrossRef](#)]